Atomic level mixing induced by Kr irradiation of Fe Co Cu multilayers

I. L. Graff, J. Geshev, S. R. Teixeira, L. Amaral, and A. Traverse

Atomic level mixing induced by Kr irradiation of FeCo/Cu multilayers

I. L. Graff,[1] J. Geshev,[1] S. R. Teixeira,[1] L. Amaral,[1,a] and A. Traverse[2]
[1]*Instituto de Física, UFRGS, CP 15051, 91501-970 Porto Alegre, Brazil*
[2]*Centre Laser Infrarouge d'Orsay-CLIO, F-91405 Orsay Cedex, France*

The effects of Kr ion irradiation of Fe_xCo_{1-x}/Cu multilayers are investigated by means of magnetic and x-ray measurements. The irradiation was performed at room temperature with 600 keV of Kr, and the fluences were ranged from 1×10^{15} to 5×10^{15} ions/cm^2. X-ray diffraction patterns show that the irradiation was able to produce a significant grain growth and, at the same time, it triggered a strain release. The x-ray absorption measurements around Fe K edge have shown that the FeCo environment changed from bcc, for the as-deposited multilayer, to fcc after appropriate fluence, depending on the Cu thickness and on the Fe/Co content. For 50 Å of Cu, the phase transformation occurs even for the lowest fluence, regardless the Fe/Co concentration. For 25 Å of Cu, it depends on the Fe/Co concentration. After irradiation, the saturation magnetization suffers a strong decrease, especially for 50 Å of Cu. The temperature for the onset of irreversibility also decreases with irradiation, again being the effect stronger for 50 Å of Cu. These data indicate that Kr irradiation induced mixing between Cu and FeCo, even though Cu is immiscible with Fe and Co in the equilibrium state. © *2008 American Institute of Physics*. [DOI: 10.1063/1.2836975]

I. INTRODUCTION

Ion irradiation of metallic multilayers can produce various effects as the energetic ion beam passes through the material. By using light ions such as He, very subtle and localized defects are produced, whereas heavy ions such as Kr or Xe form dense atomic collision cascades that produce many defects in the material. Materials submitted to heavy ion bombardment can undergo phase transformation, amorphization, intermixing, and alloying at the interface.[1] The width of the mixed layer depends on the heat of mixing, the deposited energy, and the fluence.[2–4]

The role of the heat of mixing is fundamental when we are dealing with immiscible materials. Consequently, a mixing effect can take place in a first step followed by a chemically driven demixing.[5] In this context, during the last few years, various groups produced metastable alloys between immiscible elements using ion irradiation. Yang *et al.*[6] obtained metastable phases irradiating with Xe ions the immiscible Fe–Cu system. They showed the formation of a Cu-based fcc solid solution for $Fe_{30}Cu_{70}$ composition and another fcc metastable crystalline phase for $Fe_{50}Cu_{50}$. The Co/Cu immiscible system was also investigated. Irradiation with 1 MeV Si ions produced metastable Co–Cu alloys, depending on the fluence and the thickness of the layers.[7] The predicted heats of mixing calculated with Miedema's theory[8] for Co–Cu and Fe–Cu are +10 kJ/mol (Ref. 9) and +19 kJ/mol,[10] respectively. For systems with a very strong positive heat of mixing such as, for example, Ag–Co (+28 kJ/mol),[9] irradiation induced a complete segregation of Co, forming a granular material where Co clusters are embedded in a Ag matrix.[11] The size of such Co precipitates can be controlled quite precisely by the fluence.[12]

FeCo/Cu multilayers and/or FeCo–Cu alloys have great scientific and technological interest since they present a high giant magnetoresistance (GMR) at room temperature, especially granular alloys formed after some thermal treatment.[13] The GMR effect is strongly dependent on the particle size and on the very local environment around FeCo. Therefore, it is necessary to control these two features in a precise and reliable way in order to pattern the GMR amplitude. Ion irradiation has proven to be a very precise tool that can be used to control such parameters. Besides, the FeCo alloy has a very high saturation magnetization and is commonly used in read/write magnetic heads.[14] More recently, the FeCo alloy has been employed in systems for spin-polarized current injection due to its high spin polarization at the Fermi level.[15]

Ternary Fe–Co–Cu alloys, obtained by mechanical alloying techniques, have been extensively studied by x-ray absorption spectroscopy (XAS).[16,17] The process of formation for such alloy occurs in two steps. At first, the Co and Cu become mixed, keeping the Fe in a separate phase. In the second step, after much more milling time, the Fe dissolves into the fcc lattice, thus forming a ternary solid solution. The two-step mechanism, where Co and Cu mix earlier than Fe and Cu can be attributed to the lower positive heat of mixing of the former pair of atoms. Magnetic measurements of these alloys show a ferromagneticlike behavior even for high Cu concentration.[18–21]

In order to contribute in the understanding of the ion beam mixing effect in the case of immiscible elements, we performed room temperature irradiation of FeCo/Cu multilayers with 600 keV Kr ions. Different Fe, Co, and Cu concentrations are obtained by varying the Cu thickness and (or) the relative Fe/Co amounts. The energy was chosen to assure that the ions traverse the whole multilayer, with an almost uniform energy loss profile, and going to stop deep in the substrate.

---

a)Author to whom correspondence should be addressed. Tel.: +55 51 3308 6508. FAX: +55 51 3308 7286. Electronic mail: livio.amaral@ufrgs.br.

In previous works we observed a phase transformation of the FeCo alloy from bcc to fcc after irradiation.[22–24] The goal of the present paper is to add new magnetic and structural data in order to get a complete description of the FeCo/Cu system, with two compositions of FeCo alloy, $Fe_{70}Co_{30}$ and $Fe_{30}Co_{70}$, and two Cu thicknesses, 25 and 50 Å. The structural information is obtained combining two complementary techniques, i.e., x-ray diffraction (XRD) and XAS. With XRD we obtained the lattice parameter and the mean grain size. XAS, suitable for systems with short-range order, is of fundamental importance since it provides very local information around a specific atom present in the sample. With XAS data we describe the surrounding of Fe atoms in the very thin layers. The magnetic properties and their evolution after irradiation were estimated by field cooled/zero field cooled (FC/ZFC) curves and hysteresis loops. The relationships between magnetic and structural data provide a more complete description of the system behavior.

II. EXPERIMENTAL

$[Fe_xCo_{100-x}(15\ \text{Å})/Cu(t\ \text{Å})]_{\times 10}$ multilayers were prepared by alternate e-gun evaporation of Cu and Fe_xCo_{100-x} alloy at 5×10^{-8} mbar of base pressure on oxidized Si(111) substrates. After deposition, the films were analyzed by x-ray reflectivity in order to verify if a multilayer was actually formed. The presence of Bragg peaks, together with Kiessig fringes, confirms that a multilayer was structured.[24] To minimize a possible oxidation of the FeCo alloy, a cap layer of 50 Å of Cu was deposited on the top. The evaporation was done at room temperature with less than 1 Å/s deposition rate, monitored by a computer controlled quartz microbalance. Four samples were prepared using two thicknesses of Cu, $t=25$ and 50 Å, and two concentrations of Fe, $x=30\%$ and 70%. The ion irradiation was carried out at room temperature with 600 keV Kr^+ and fluences ranging from 1×10^{15} to 5×10^{15} ions/cm^2. The current density during irradiation was kept at 100 nA/cm^2 to avoid heating of the sample. Using the SRIM code,[25] we calculated that with this incident energy and for the thickest configuration (50 Å of Cu), the projected range of the Kr ions is around 1600 Å, i.e., they traverse the whole multilayer and stop in the substrate. The energy loss profile of the ions is rather constant in the multilayer, showing only a very small increase from the impinging position until the end of the multilayer.

The structural characterization of the samples was done using XRD and XAS. X-ray diffraction patterns were obtained in a Bragg–Brentano geometry using a Cu $K\alpha$ radiation source. All samples were submitted to the same scanning procedure for comparison purpose. The scanning range was between 35° and 55° in 2θ, since this range contains the most intense peaks for Cu and FeCo.

The XAS measurements were performed at the Co, Fe, and Cu K edges using the XAFS1 beam line facility of the Laboratório Nacional de Luz Síncrotron (LNLS)[26] and the XAS beam line at ELETTRA Synchrotron.[27] The samples were measured in fluorescence and total electron yield modes, with the x-ray beam polarization vector in the plane

of the samples. The XAS data reduction and analysis followed standard procedures, well described in the literature,[28] using ATHENA and ARTEMIS software packages.[29] The range in wave vector space used in the analysis was between 3 and 12 Å^{-1}. The backscattering and phase functions necessary for the fittings were theoretically calculated with FEFF6 code.[30]

FC/ZFC curves were acquired using a superconducting quantum interference device (SQUID) from Quantum Design, between 10 and 300 K. The applied magnetic field during the measurements was 100 Oe. Hysteresis loops at room temperature were obtained by means of an alternating gradient force magnetometer (AGFM). In order to get information about the magnetic behavior evolution of the samples, magnetization data were obtained before and after irradiation.

III. RESULTS

A. X-ray diffraction (XRD)

Figure 1 shows the diffraction patterns for the $[Fe_xCo_{100-x}(15\ \text{Å})/Cu(t\ \text{Å})]_{\times 10}$ multilayers before and after irradiation. All patterns for the as-deposited samples exhibit only one broad peak with low intensity around $2\theta=44°$, which is attributed to Cu(111). The 2θ value is larger than the expected for bulk Cu one and is slightly different from one sample to another. After irradiation, the Cu(111) linewidth decreases and the intensity enhances a lot. Irradiation also pushes the Cu(111) peak position to lower angles, closer to the bulk value (43.31°). As it is clearly noted in Fig. 1, the displacement depends on the Fe/Co concentration and Cu thickness. Another peak, attributed to Cu(200), can be clearly identified after 1×10^{15} ions/cm^2 for cases of Figs. 1(b) and 1(d) growing with the fluence, whereas it remains small for cases of Figs. 1(a) and 1(c). The Cu(200) intensity never reaches the expected intensity for a polycrystalline sample.

It is important to note that there is no clear indication for the FeCo(110) peak in the as-deposited samples; this peak is expected to be located just at the right-hand side of the Cu(111) peak. After irradiation, it is possible to identify the FeCo(110) peak only for the sample of case (c).

The mean grain size of the samples was obtained by fitting the diffraction peaks with a pseudo-Voigt profile function and extracting the linewidth and position. Subsequently, we used the Scherrer equation[31] to calculate the grain size. However, this equation was derived for very small particles, free of strain and faulting. Since it is probably not the case of our samples, the equation is used only to give a rough estimation of the grain size, keeping in mind that strain and faulting effects were not taken into account.

The lattice parameter a and the mean grain size $\langle D \rangle$ calculated from the Cu(111) position as a function of the fluence are presented in Fig. 2. All as-deposited samples present a lattice parameter smaller than the bulk one, meaning that Cu is compressed, the compression depending on Cu thickness and Fe/Co concentrations [Fig. 2(a)]. The Cu lattice is more compressed for smaller Cu thickness. Submitted to ion irradiation, the samples release strain and the lattice parameter attains the bulk Cu value for the $Fe_{70}Co_{30}(15\ \text{Å})/Cu(50\ \text{Å})$ and $Fe_{70}Co_{30}(15\ \text{Å})/Cu(25\ \text{Å})$ films. In the samples with
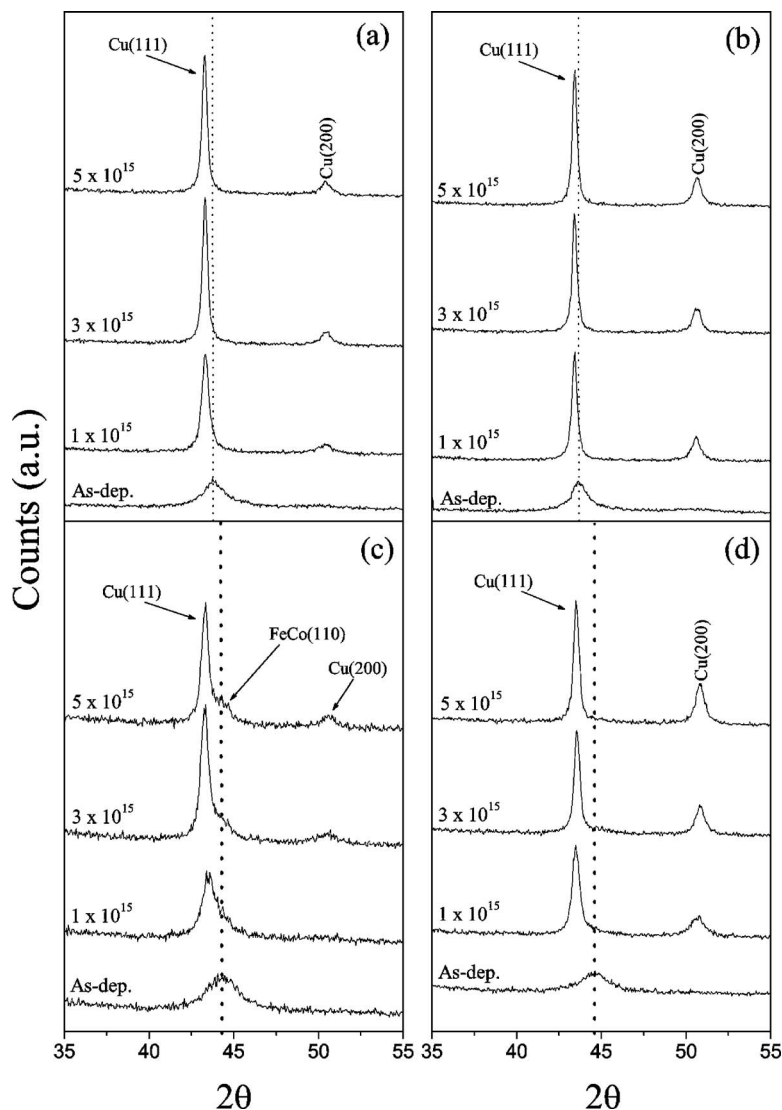
FIG. 1. X-ray diffraction patterns for the multilayers before and after irradiation. (a) $Fe_{70}Co_{30}$(15 Å)/Cu(50 Å), (b) $Fe_{30}Co_{70}$(15 Å)/Cu(50 Å), (c) $Fe_{70}Co_{30}$(15 Å)/Cu(25 Å), and (d) $Fe_{30}Co_{70}$(15 Å)/Cu(25 Å). The irradiation fluences are shown in the figures, 1×10^{15}, 3×10^{15}, and 5×10^{15} ions/cm². The vertical dashed line serves as reference to follow the peak displacement after irradiation.

higher Co concentration, the lattice parameter does not reach the Cu bulk value, which shows clearly the dependence of the structural evolution on the Fe/Co content.

The grain size of Cu for the as-deposited samples is about 50 Å and experiences a big enhancement with ion fluence, reaching around 250 Å as the maximum value [Fig. 2(b)]. However, sample $Fe_{70}Co_{30}$(15 Å)/Cu(25 Å) does not follow the same dynamics of the other ones. The maximum grain size attained in that case is around 170 Å, for 5 $\times 10^{15}$ ions/cm². Note that only information concerning the Cu evolution is provided by XRD since no FeCo diffraction peak was detected.

B. X-ray absorption spectroscopy (XAS)

1. Qualitative considerations

XAS measures the absorption coefficient (μ) of a given material as a function of the incident photon energy. The oscillatory structure that appears in the absorption coefficient just above the absorption edge turns out to be an unique signature of the material.[32] These oscillations depend on the detailed atomic structure as well as on the electronic and vibrational properties. As XAS is chemical selective, i.e., the

incident energy can be tuned and scanned around a specific absorption edge, it is a very important probe of materials. Also, XAS is by excellence a short-range order technique, which is a fundamental feature when we are dealing with nanometer scale systems.

Figure 3 shows the extended x-ray absorption fine structure (EXAFS) signals for the Fe_xCo_{100-x}(15 Å)/Cu(tÅ) multilayers at the Fe K edge. With the XAS technique, we are able to look around Fe atoms and to characterize in details their structural evolution after irradiation. Measurements around Co K edge were also done and the overall structural evolution of the signals is qualitatively the same as for Fe K edge. So, for the sake of simplicity, we have chosen to present only the Fe K-edge results. Around Cu, XAS data have revealed a fcc structure in the as-deposited sample and remains fcc after irradiation without any appreciable modification. Therefore, we have omitted data referent to Cu K edge to drive our attention to the evolution of Fe K edge. In Fig. 3(b) we show only the as-deposited and 3 $\times 10^{15}$ ions/cm² irradiated samples' signals. This specific sample was studied in a previous work[22] and follows the same behavior as that shown in Fig. 3(a).
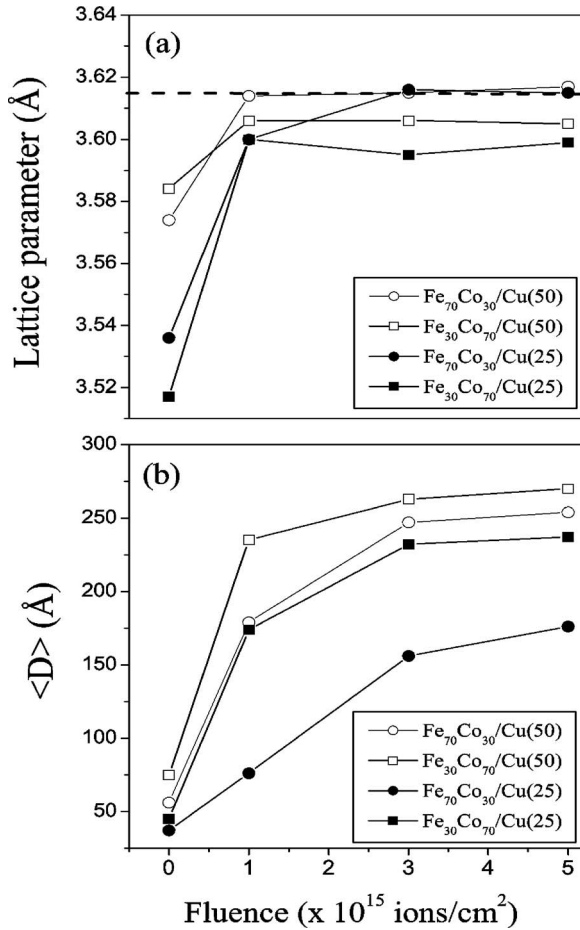
FIG. 2. Lattice parameter a (a) and the mean grain size $\langle D \rangle$ (b) as a function of ion fluence obtained from Cu(111) peak. The dashed line in (a) is just a reference line indicating the bulk value for Cu (3.615 Å).

FIG. 3. (Color online) EXAFS signals at Fe K edge for the multilayers before and after irradiation. (a) $Fe_{70}Co_{30}(15$ Å$)/Cu(50$ Å$)$, (b) $Fe_{30}Co_{70}(15$ Å$)/Cu(50$ Å$)$, (c) $Fe_{70}Co_{30}(15$ Å$)/Cu(25$ Å$)$, and (d) $Fe_{30}Co_{70}(15$ Å$)/Cu(25$ Å$)$. The signals for Cu and Fe references are shown for comparison purposes. The arrows indicate two features of a bcc structure.

In the as-deposited state the FeCo layers, whatever the Cu thickness and Fe/Co concentration, have a bcc structure, as seen by comparison to the Fe reference signal. This agrees with the equilibrium phase diagram for FeCo.[33] The main difference between the as-deposited samples and the Fe reference foil concerns to the amplitude of the signals, that is much lower for the multilayers.

The irradiated samples evolve to another structure. Comparing the new structure to the fcc Cu reference signal, also shown in the Fig. 3, it is possible to assert that the irradiated sample's signals are characteristic of a fcc structure. The exception is $Fe_{70}Co_{30}(15$ Å$)/Cu(25$ Å$)$ sample [Fig. 3(c)], where a different behavior is observed. The initial bcc structure is not completely transformed after irradiation (see the arrows in the figure).

The Fourier transforms (FTs) of the EXAFS signals can also give insight about the structure of the samples. They represent the radial distribution of atoms around a specific absorber (unless phase correction), the peaks originating from different atomic shells. The FTs at Fe K edge of the EXAFS signals, weighted by k, are shown in Fig. 4. There, we can see the same behavior for the structural evolution as observed with the EXAFS signals. In case of Figs. 4(a), 4(b), and 4(d), we note that the shape of the as-deposited FT evolves after irradiation, becoming quite similar to the FT of
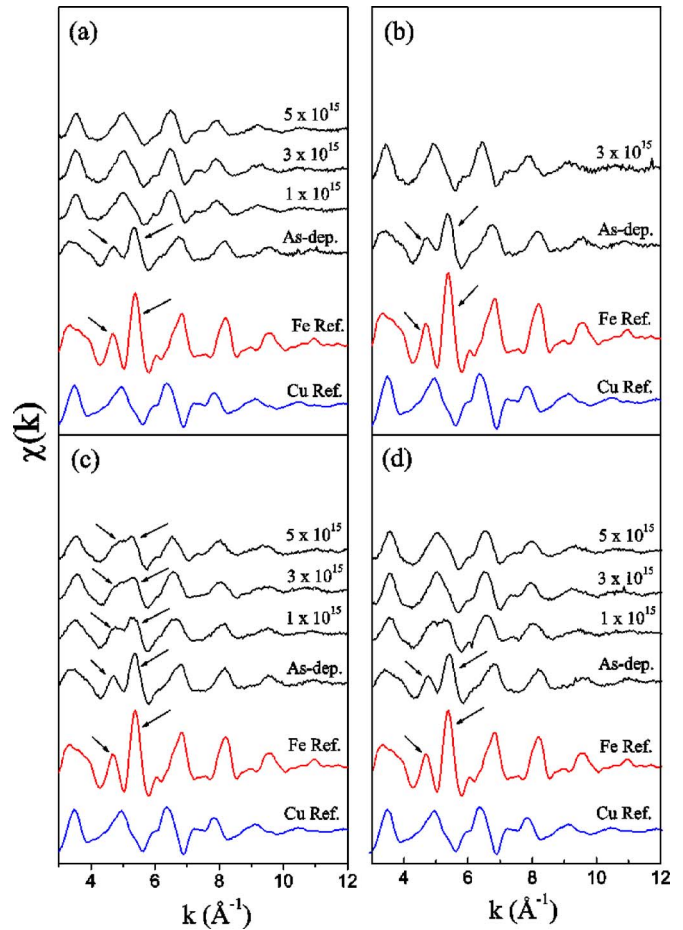
the Cu reference. This is clear especially when we compare the region between 3 and 6 Å for the samples and Cu reference FT. In Fig. 4(c) the evolution of the FT follows a different way, being the irradiation unable to completely transform the structure. For 50 Å of Cu, the phase transition happens even for the lowest fluence, 1×10^{15} ions/cm^2, which shows the influence of the Cu thickness. In contrast, for 25 Å of Cu, the phase transformation occurs for higher fluences, if any, and strongly depends on the Fe/Co content.

2. Quantitative results

In order to obtain quantitative information, we have fitted the back-transformed first peak of the FT, i.e., the fitting is done in k space. The fittings provided the number of first neighbors N_j, distance of first neighbors R_j, and the Debye-Waller factors σ_j^2 for each atomic shell. The first peak of the FT originates, in general, from the first atomic shell around the absorbing atom. Therefore, by fitting this peak we get atomic-level information, i.e., the very local order around a specific atom. To effectuate the fittings the as-deposited sample was described as a bcc structure based on the observations from EXAFS. In the bcc structure for FeCo (and Fe), the two first atomic shells are very close together, 2.46 and
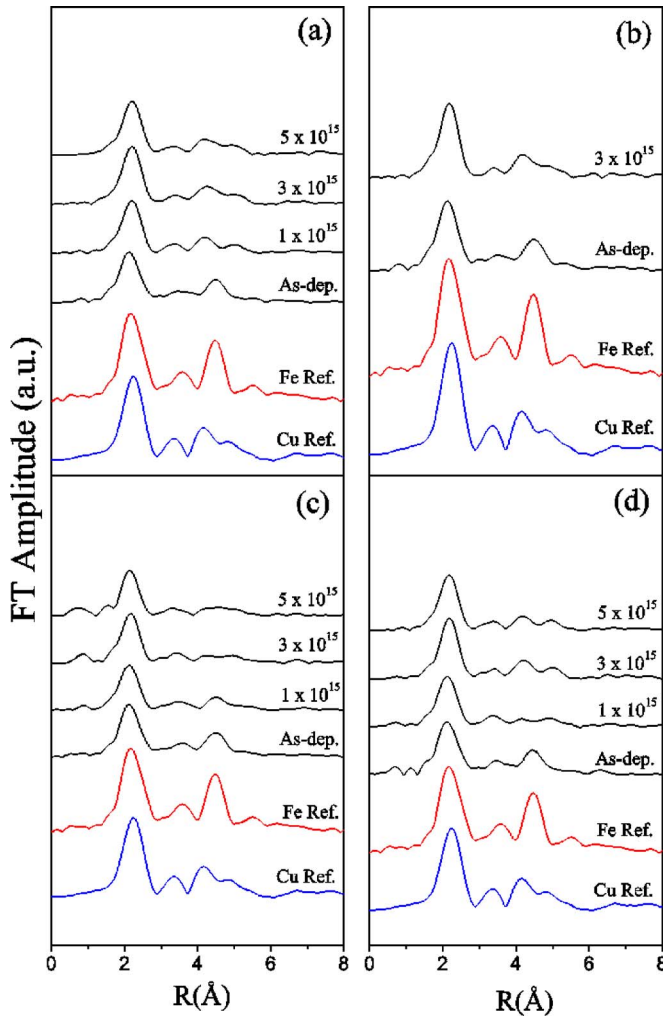
FIG. 4. (Color online) Fourier transforms (FT) amplitudes at Fe K edge of the weighted EXAFS signals $[k\chi(k)]$. (a) $Fe_{70}Co_{30}(15 \text{ Å})/Cu(50 \text{ Å})$, (b) $Fe_{30}Co_{70}(15 \text{ Å})/Cu(50 \text{ Å})$, (c) $Fe_{70}Co_{30}(15 \text{ Å})/Cu(25 \text{ Å})$, and (d) $Fe_{30}Co_{70}(15 \text{ Å})/Cu(25 \text{ Å})$. The FT for Cu and Fe references are shown for comparison purposes.

2.84 Å, with 8 and 6 neighbors, respectively. Because the Fe EXAFS has a limited R-space resolution of $\Delta R \approx 0.4$ Å, the first peak of the FT is originated from the two first atomic shells. Thus, the fitting for the as-deposited samples has been done considering two atomic shells for the first peak. The backscattering and phase functions used in the fittings were calculated for a bcc ordered FeCo alloy using the FEFF6

code.[30] For the ordered structure, the first eight neighbors of Fe are Co atoms and the second neighbors are six Fe atoms.

The obtained parameters are shown in Table I for the as-deposited samples at Fe K edge. The two distances shown in this table are consistent with a bcc structure, as suggested before. The number of first neighbors is systematically smaller than in a bulk well-organized bcc crystalline structure, which may be an effect of the film growth process.[34] Stacking faults can be produced during the film growth, which results in vacant sites and reduces the effective number of neighbors. Also, the model used in the simulation supposes an ordered bcc structure of FeCo. However, the FeCo layers probably are not ordered, with the alloy being a disordered structure (solid solution). A typical fitting curve for the as-deposited samples is shown in Fig. 5(a). As can be observed, the fitting is quite good and the resulting $\mathfrak{R}$ factor is very small. The $\mathfrak{R}$ factor gives a sum-of-squares measure of the fractional misfit[35] between data and theory, and can be used to evaluate the goodness of a fit. In principle, we can be confident that any fit that results in $\mathfrak{R} \leq 0.02$ is acceptable.

In Table II we present the values obtained by fitting the samples irradiated with 3×10^{15} ions/cm^2, that is, the fluence where a complete bcc to fcc phase transformation was observed by EXAFS signals. Two models were built up in FEFF6 code to theoretically calculate EXAFS signals, phase, and backscattering functions. The theoretical curves were fitted against the experimental ones and the results were used to check if mixing had occurred.

- Model 1: 12 Fe scattering atoms as first neighbors around a central Fe absorbing atom, at 2.55 Å distance.
- Model 2: six Fe and six Cu scattering atoms as first neighbors around a central Fe absorbing atom, at an initial distance of 2.55 Å.

With model 1 we tried to simulate a Fe-pure fcc cluster embedded in Cu matrix. Model 2 simulates Fe and Cu mixed at an atomic level. All parameters (R_j, N_j, and σ_j^2) were let free to vary, with the constrain condition for model 1, $N_{Fe} \leq 12$, and for model 2, $N_{Fe} + N_{Cu} \leq 12$. Special care is implemented to ensure that the maximum number of fitting parameters never exceeded the number of relevant independent data points, which is given by[36] $N_{ind} = 2\Delta k \Delta R/\pi + 2$. Δk and ΔR are the ranges of the Fourier transform in k and R spaces, respectively. In our case, $\Delta k \approx 9$ Å^{-1} and $\Delta R \approx 2$ Å, which

TABLE I. Structural parameters obtained from fitting the back-transformed first peak of the Fourier Transforms for the as-deposited multilayer at Fe K edge. (A) $Fe_{70}Co_{30}(15 \text{ Å})/Cu(50 \text{ Å})$, (B) $Fe_{30}Co_{70}(15 \text{ Å})/Cu(50 \text{ Å})$, (C) $Fe_{70}Co_{30}(15 \text{ Å})/Cu(25 \text{ Å})$, and (D) $Fe_{30}Co_{70}(15 \text{ Å})/Cu(25 \text{ Å})$. The backscattering and phase functions were calculated by FEFF6 for an ordered FeCo (bcc) alloy with Fe as absorber at the center of the cluster.

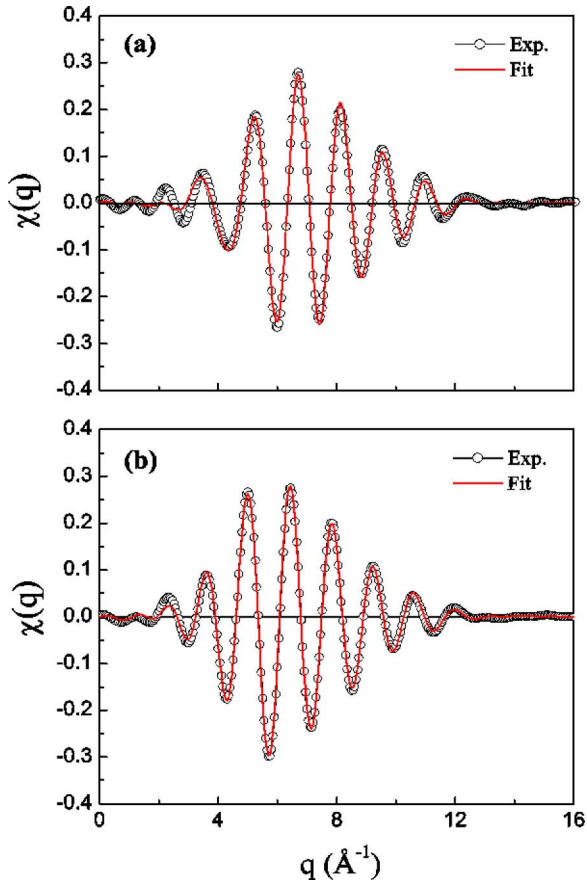| Sample	(A)	(B)	(C)	(D)	Fe Ref.
N_{Fe-Co}	5.7(0.52)	6.0(0.65)	5.4(0.40)	6.0(0.54)	8
N_{Fe-Fe}	4.5(1.13)	5.0(1.61)	5.2(1.21)	5.3(1.34)	6
R_{Fe-Co} (Å)	2.45(0.02)	2.46(0.01)	2.46(0.01)	2.45(0.02)	2.47
R_{Fe-Fe} (Å)	2.82(0.03)	2.83(0.02)	2.84(0.01)	2.83(0.02)	2.83
σ_{Fe-Co}^2 (Å^2)	0.0067(0.0008)	0.0068(0.001)	0.0056(0.0006)	0.0058(0.0008)	⋯
σ_{Fe-Fe}^2 (Å^2)	0.0112(0.003)	0.0131(0.004)	0.0142(0.003)	0.0120(0.003)	⋯
$\mathfrak{R}$ factor (%)	0.7	0.8	0.4	0.6	⋯

FIG. 5. (Color online) Two typical fittings of the back-transformed first peak of the FT obtained for (a) $Fe_{70}Co_{30}(15 \text{ Å})/Cu(50 \text{ Å})$ as deposited and (b) $Fe_{70}Co_{30}(15 \text{ Å})/Cu(50 \text{ Å})$ irradiated with 3×10^{15} ions/cm².

results in $N_{ind} \approx 13$. Last but not the least, it is important to note that the phase functions for Fe and Cu are sufficiently different to distinguish one atom from another, as was already shown before by Harris *et al.*[37]

The best fits are obtained for model 2 as verified by comparing the $\mathfrak{R}$ factors (see Table II). Note that the number of Cu atoms in the first atomic shell is always much larger than that of Fe atoms. This can be attributed to the much higher concentration of Cu in the multilayers. When Fe, Co, and Cu become mixed, they will form a ternary solid solu-

tion where the majority of the lattice sites are occupied by Cu atoms. In the fittings, the Co atoms were not introduced since Co and Fe atoms are indistinguishable from the point of view of EXAFS. The phase and backscattering functions for Fe–Co and Fe–Fe atom pairs, as calculated by FEFF56,[30] are almost identical.

As can be noted, the data for the irradiated samples with 25 Å thick Cu layers are not shown in Table II. In that case, the fitting results were not reasonable from the physical point of view. The minimization procedure of ARTEMIS code[29] resulted in negative values for first neighbors and Debye–Waller factors, which has no sense. Probably, such results are due to the fact that, for 25 Å of Cu, the structure is not completely transformed, being constituted by locally mixed regions together with separated ones. In such case, the assumed fitting models are not appropriate to describe the structure.

C. Magnetic measurements

1. Hysteresis loops

Figure 6 gives the AGFM hysteresis loops measured for magnetic field applied in the samples' plane at room temperature. These show predominantly ferromagnetic behavior, where the rounded shape near remanence and the absence of in-plane anisotropy indicate that the systems consist of disordered fine particles. The anisotropy of the samples, which hysteresis loops are plotted in Figs. 6(b) and 6(d), is approximately twice higher than that of the samples which curves are plotted in Figs. 6(a) and 6(b). The values of the coercive field (H_c) are larger for samples with higher Co content or, in other words, the samples with lower Fe concentration are magnetically harder. The saturation magnetization (M_s), which is directly correlated to the magnetic moment, is strongly dependent on the Cu thickness in the multilayers. M_s is smaller for 50 Å of Cu than for 25 Å (see figure). Also, in the former case [Figs. 6(a) and 6(b)], M_s is larger for sample with less Co content, i.e., 1800 emu/cm³ for $Fe_{70}Co_{30}$ and 1400 emu/cm³ for[38] $Fe_{30}Co_{70}$. In the case of 25 Å of Cu [Figs. 6(c) and 6(d)], M_s is around 1960 emu/cm³ and does not change with Co concentration.

TABLE II. Structural parameters obtained from fitting the back-transformed first peak of the Fourier transforms for irradiated samples at Fe K edge. (A) $Fe_{70}Co_{30}(15 \text{ Å})/Cu(50 \text{ Å})$ and (B) $Fe_{30}Co_{70}(15 \text{ Å})/Cu(50 \text{ Å})$. The backscattering and phase functions were calculated by FEFF6 supposing two models, as described in the text, with Fe as absorber at the center of the cluster.

	N_{Fe-Fe}	N_{Fe-Cu}	$\mathfrak{R}$ (Å)	σ^2_{Fe-Fe} (Å²)	σ^2_{Fe-Cu} (Å²)	$\mathfrak{R}$ factor (%)
			(A)			
Model 1	5.7(0.4)	⋯	2.56(0.002)	0.006(0.00067)	⋯	0.5
Model 2	2.0(1.2)	7.3(3.7)	2.54(0.013)	0.013(0.02)	0.009(0.0008)	0.06
			(B)			
Model 1	5.6(0.7)	⋯	2.56(0.0002)	0.006(0.0012)	⋯	1.6
Model 2	2.2(1.8)	7.08(3.0)	2.54(0.015)	0.013(0.03)	0.009(0.001)	0.1
Cu Ref.	N_{Cu-Cu}		R (Å)		σ^2_{Cu-Cu} (Å²)	
	12	⋯	2.55	⋯	⋯	⋯

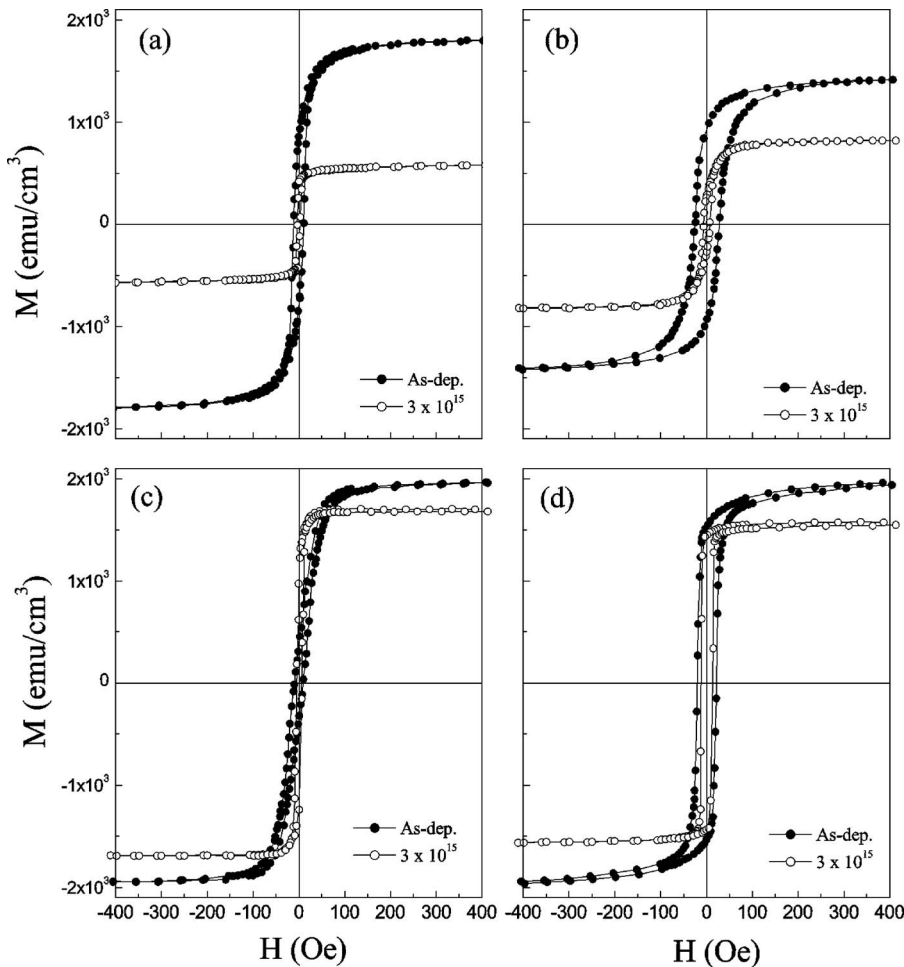FIG. 6. Hysteresis loops for the as-deposited and irradiated with 3×10^{15} ions/cm^2 multilayers. (a) Fe$_{70}$Co$_{30}$(15 Å)/Cu(50 Å), (b) Fe$_{30}$Co$_{70}$(15 Å)/Cu(50 Å), (c) Fe$_{70}$Co$_{30}$(15 Å)/Cu(25 Å), (d) Fe$_{30}$Co$_{70}$(15 Å)/Cu(25 Å).

One notes two main differences between the hysteresis loops' characteristics of the as-deposited and irradiated samples, for 50 Å of Cu. These are as follows: (i) after irradiation, the saturation magnetization decreases significantly, e.g., approximately 70% in Fig. 6(a) and 42% in Fig. 6(b); (ii) the coercive field decreases showing that irradiation also reduces the in-plane anisotropy.

The samples with 25 Å of Cu [Figs. 6(c) and 6(d)] did not show very significant decreases of M_s and H_c after irradiation.

The more detailed analysis of the hysteresis loops measured for all as-deposited samples indicates that they are composed of two types of magnetic particles. The nonzero slope of the magnetization curves at high fields is a characteristic of superparamagnetic (SPM) contribution. The noticeable "tail," also typical of these curves (i.e., the descending and ascending branches of a loop stay close together but do not coincide for a broad field range), indicates that there is a distribution in size or in shape of the ferromagnetic (FM) particles, which form the other magnetic phase of these systems.

The above observations are illustrated in Fig. 7, where the experimental hysteresis loop for the as-deposited multilayer with composition [Fe$_{70}$Co$_{30}$(15 Å)/Cu(50 Å)]$_{\times 10}$ is shown along with the corresponding best-fitting curve. The solid line, fitting the experimental data (solid circles), is a sum of the two curves plotted in the inset. These are SPM and FM components, the latter being a weighted average of curves calculated as explained below, using Gaussian anisotropy field distribution with mean value of 26 Oe and standard deviation of 8.6 Oe. As a basis for the calculation of the FM part of this fitting curve, we used a hysteresis loop simulated in the framework of the Stoner–Wohlfarth model[39] for a
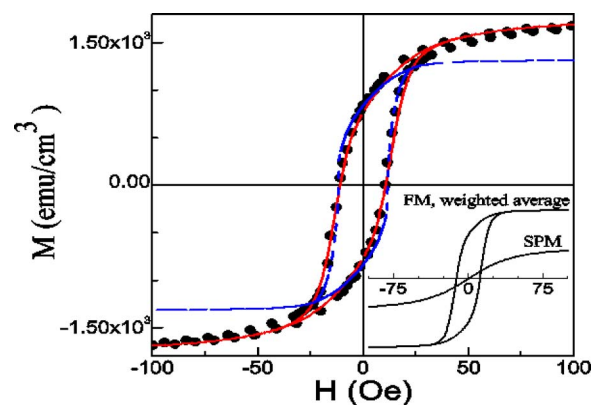

FIG. 7. (Color online) Best fitting of the hysteresis loop for the as-deposited multilayer with composition [Fe$_{70}$Co$_{30}$(15 Å)/Cu(50 Å)]$_{\times 10}$. The solid line (red), fitting the experimental data (solid circles), is a sum of the two curves plotted in the inset. These are superparamagnetic (SPM) and ferromagnetic (FM) components, the latter being a weighted average of curves calculated as explained in the text, using Gaussian anisotropy field distribution with mean value of 26 Oe (corresponding to the dashed line in the figure) and standard deviation of 8.6 Oe.
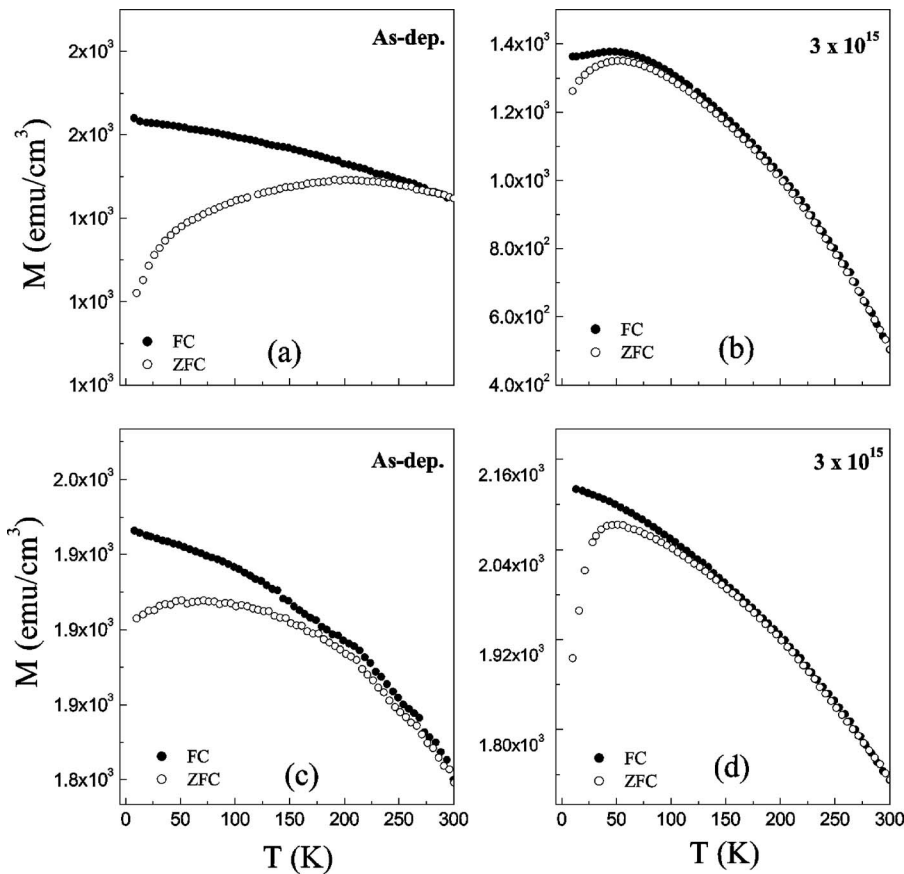
FIG. 8. FC/ZFC curves for the as de-posited and irradiated with 3 $\times 10^{15}$ ions/cm^2 multilayers. Top panel: Fe$_{70}$Co$_{30}$(15 Å)/Cu(50 Å) (a) as deposited and (b) irradiated. Bottom panel: Fe$_{70}$Co$_{30}$(15 Å)/Cu(25 Å) (a) as deposited and (b) irradiated. The dc applied field during the measurements was 100 Oe.

disordered system of noninteracting single-domain particles with uniaxial anisotropy, assuming that their easy magneti-zation axes are randomly distributed in the plane of a film. The uniaxial anisotropy could be, e.g., due to the elongated shape of the particles (in materials with cubic anisotropy constant much lower than M_s^2, such as Fe and Co, the shape, i.e., uniaxial anisotropy, predominates over the cubic one[39]). Thus calculated hysteresis loop is given in Fig. 7 by the dashed line. Details on the calculation procedure are given elsewhere.[40]

There is a very good agreement between model and ex-periment, as can be seen in the figure, confirming the pres-ence of SPM and FM particles, the latter with a certain an-isotropy field distribution. The shapes of the hysteresis loops of the irradiated samples, however, show no traces of SPM phase. This can be associated with an increase of the small-sized SPM particles after irradiation. On the other hand, the decrease of H_c after irradiation shows that the effective an-isotropy field is decreased. Thus, the irradiation effectively narrows the anisotropy field distribution, by changing the size (or the shape) of the grains.

2. FC/ZFC curves

The temperature dependence of the magnetization is shown in Figs. 8 and 9. Figure 8 presents the FC/ZFC curves for Fe$_{70}$Co$_{30}$(15 Å)/Cu(25 Å) and Fe$_{70}$Co$_{30}$(15 Å)/ Cu(50 Å) samples. The curves for the as-deposited samples (panels a and c) are characteristic of a film which consists of grains with broad anisotropy field distribu-tion. The very wide cusp of the corresponding ZFC curves and the high collapse temperatures of the ZFC and FC curves evidence this observation.[41] Such a high temperature for the onset of irreversibility, around 250 K, confirms that the ef-fective magnetic volume of the grains is big.

After irradiation, the FC/ZFC curves change signifi-cantly for the sample with 50 Å of Cu [see Fig. 8(b)]. The temperature for the onset of irreversibility goes down to val-ues around 50 K, indicating that irradiation promoted an im-portant reduction of the effective magnetic grain size. Also, it seems that the Curie temperature (T_c), which is well above room temperature for the as-deposited sample, decreases af-ter irradiation.[42] For 25 Å of Cu, the evolution of the curves is less pronounced, which, once again, confirms that irradia-tion narrows the mean anisotropy field distribution in this case.

Figure 9 shows the FC/ZFC curves for Fe$_{30}$Co$_{70}$(15 Å)/Cu(25 Å) and Fe$_{30}$Co$_{70}$(15 Å)/Cu(50 Å) samples. The overall behavior of these samples is similar to that shown in Fig. 8. However, the as-deposited curves are characteristic of grains with much narrower anisotropy field distribution as compared with those plotted in Figs. 8(a) and 8(c), since the FC magnetization varies only few percent over the whole temperature range. The irradiation affects mainly the sample with 50 Å of Cu, reducing the tempera-ture for the onset of irreversibility as well as T_c. The differ-ences between the curves before and after the irradiation for the sample with 25 Å of Cu are less pronounced as com-pared to the case of 50 Å of Cu.
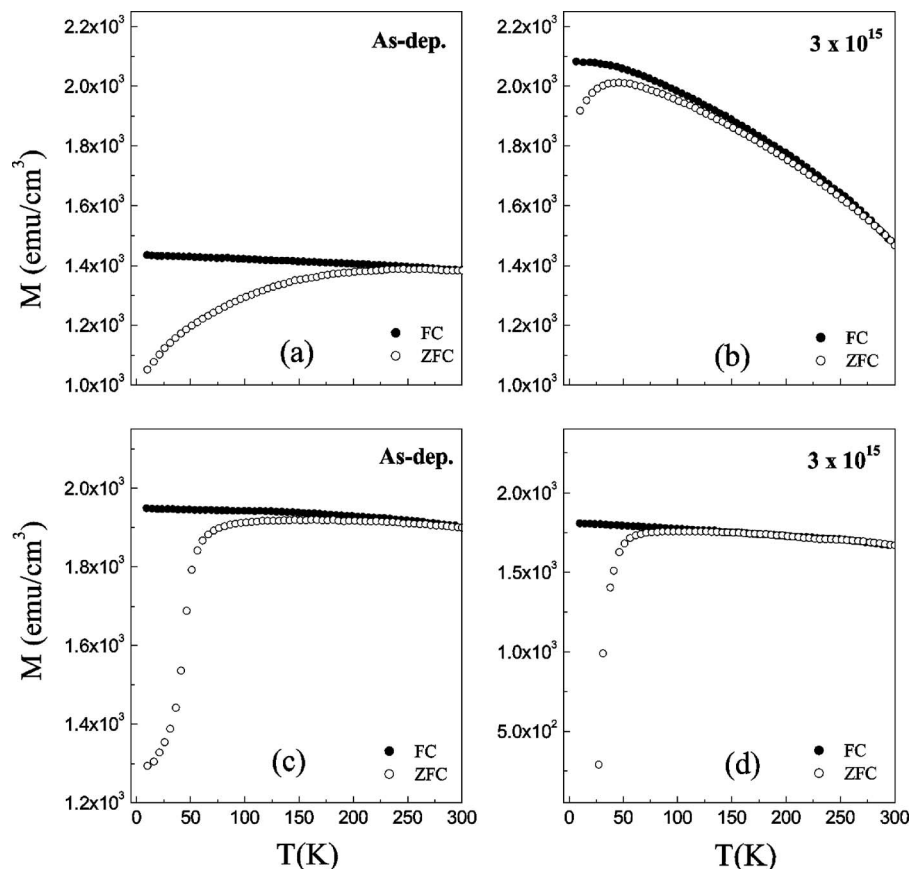
FIG. 9. FC/ZFC curves for the as deposited and irradiated with 3×10^{15} ions/cm^2 multilayers. Top panel: Fe$_{30}$Co$_{70}$(15 Å)/Cu(50 Å) (a) as deposited and (b) irradiated. Bottom panel: Fe$_{30}$Co$_{70}$(15 Å)/Cu(25 Å) (a) as deposited and (b) irradiated. The dc applied field during the measurements was 100 Oe.

IV. DISCUSSION

A. As-deposited samples

The structure of the FeCo layers is bcc in the as-deposited multilayer. There are no peaks in XRD patterns for the FeCo layers, probably due to the large width of the Cu(111) peak and the small quantity of FeCo, in comparison to Cu. The structure of FeCo for the as-deposited multilayers was confirmed by XAS, either qualitatively by direct comparison to standards or quantitatively by fittings. The as-deposited samples are ferromagnetic with an easy-plane anisotropy, which is higher for the samples with more Co. The ratio between the remanent and saturation magnetizations is also greater for samples with higher Co concentration, which may indicate that the particles in these samples interact ferromagnetically. The slower approach to saturation for samples with less Fe may be due to superparamagnetic grains, dispersed around each FeCo layer, as discussed above.

B. Irradiated samples

Ion irradiation induces Cu grain growth and triggers a strain release, the final lattice parameter value being slightly different from one sample to the other. Some texture is present in the final stack, as estimated by the Cu(200)/Cu(111) intensity ratio. The FeCo alloy undergoes a bcc to fcc structural transition depending on the Cu thickness and Fe concentration. For 50 Å of Cu, the structural transformation is indifferent to Fe content, taking place even for the lowest fluence. However, for 25 Å of Cu, the transformation

depends on the Fe concentration. When the samples contain more Fe, the transition has a higher energetic cost, which retards the transformation.

The evolution of the Cu lattice parameter after irradiation also depends on the quantity of Fe present in the sample (see Fig. 2). Samples with higher Fe content attain the bulk value for Cu, contrary to the ones with lower concentration. The grain size follows a dynamics that also depends on Fe, with the growth of size being faster for the samples with less Fe. Besides, higher values of grain size are reached when more Co is present. It is important to note that the XRD peak assigned as Cu(111) probably refers to the (111) peak of the fcc Fe–Co–Cu ternary alloy, formed by the irradiation. In such case, the grain size corresponds to the grain of the solid solution, which is not only constituted by Cu.

The correlation between the final Cu lattice parameter and the Co concentration may be related to the introduction of Co atoms in the Cu lattice through ion beam mixing effect. The atomic size of Co is smaller than that of Cu, and the introduction of Co in the Cu structure effectively decreases the lattice parameter, a similar effect that was observed in mechanical alloying experiments.[18,19]

The magnetization data clearly agree with results and conclusions drawn from the structural data. In the case of 50 Å of Cu, M_s decreases significantly after irradiation. Since it is an intrinsic property of the material which does not depend on grain size,[39] the strong reduction of M_s can be explained by a change of chemical environment of FeCo, i.e., mixing of Fe and Co with Cu. T_c, also an intrinsic property, seems to decrease after irradiation indicating that the

local environment of FeCo has changed. In case of 25 Å of Cu, M_s and T_c are practically unaffected by the irradiation, which confirms the dependence of the transformation on Cu thickness. The shape of the hysteresis loops after irradiation is characteristic of a ferromagnetic material. Therefore, the formation of small FeCo superparamagnetic grains with fcc structure embbeded in a Cu matrix can be ruled out.

Actually, the phase transition can be explained through a process of dissolution of the Fe and Co atoms into the fcc Cu lattice. Even though (i) the elements are immiscible in equilibrium conditions and (ii) mixing efficiency is expected to be small for the chosen energy, the energy transmitted by the ions directly to the target atoms may induce mixing. Once mixed, the free energy coming from the positive heat of mixing (ΔH_m) between the elements, Cu–Fe and Cu–Co, is not sufficient to drive back the mixture to the original atomically separated state, as seen, for instance, in the case of Co–Ag.[11]

As discussed above, Co and Fe are not equivalent in the mixing process. So, remembering that ΔH_m for Co–Cu is about twice smaller than for Fe–Cu,[9,10] one should expect that Co mixes with Cu easier than Fe. A crude picture of the mixing process is proposed. The energy deposited by Kr irradiation breaks up the Fe, Co, and Cu atomic bonds, since the energy of the incident ions is some orders of magnitude larger than the bonding energy in the solid. The atoms are displaced from their lattice sites and are randomly distributed. In a second step, they will recombine and form a ternary compound, assuming the crystalline structure of the major constituent, i.e., Cu. As ΔH_m for Co–Cu is half smaller than ΔH_m for Fe–Cu, Co will mix faster and/or easier with Cu than Fe.

It is worthwhile to note that ion irradiation was used to produce ternary alloys of Fe–Co–Cu. Such alloys were obtained by other groups through ball milling experiments.[16–21] As long as the authors know, these ternary alloys were for the first time obtained by ion irradiation experiment. Ion irradiation has some advantages in comparison to ball milling, i.e., precise control of ion fluence, current, and temperature, being the experiment carried out in high vacuum. All these features are quite important to obtain reliable and low-impurity concentration materials.

V. CONCLUSIONS

In conclusion, we have observed (i) a strain release and a huge grain growth for Cu, (ii) a bcc to fcc phase transition for FeCo in the Fe_xCo_{100-x}(15 Å)/Cu(t Å) multilayers, and (iii) a decrease of saturation magnetization and coercive field, after Kr irradiation. The Fe, Co, and Cu atoms show a tendency to become mixed after irradiation, especially for the samples with 50 Å of Cu. For 25 Å of Cu, the mixing effect critically dependents on Fe concentration. These differences can be explained by means of the heat of mixing. The heat of mixing amplitude for Fe–Cu is about twice higher than that for Co–Cu, imposing in such way a higher energy barrier to the transformation. The magnetic and structural data support the idea that a fcc Fe–Co–Cu ternary alloy was obtained through ion irradiation, even being the elements immiscible in equilibrium conditions.

[1] M. Nastasi and J. W. Mayer, Mater. Sci. Eng., R. **12**, 1 (1994).
[2] Y.-T. Cheng, Mater. Sci. Rep. **5**, 45 (1990).
[3] A. Paesano, Jr., S. R. Teixeira, and L. Amaral, J. Appl. Phys. **70**, 4870 (1991).
[4] A. T. Motta, A. Paesano, Jr., R. C. Birtcher, M. E. Brückmann, S. R. Teixeira, and L. Amaral, J. Appl. Phys. **85**, 7146 (1999).
[5] M. Nastasi and J. W. Mayer, Mater. Sci. Rep. **6**, 1 (1991).
[6] G. W. Yang, W. S. Lai, and X. Liu, J. Appl. Phys. **87**, 7232 (2000).
[7] M. Cai, T. Veres, S. Roorda, F. Schiettekatte, and R. W. Cochrane, J. Appl. Phys. **95**, 1996 (2004); **95**, 2006 (2004).
[8] A. R. Miedema, Philips Tech. Rev. **36**, 217 (1976).
[9] A. K. Niessen, A. R. Miedema, F. R. de Boer, and R. Boom, Physica B & C **151**, 401 (1988).
[10] R. Boom, F. R. de Boer, A. K. Niessen, and A. R. Miedema, Physica B & C **115**, 285 (1983).
[11] T. Veres, M. Cai, R. W. Cochrane, and S. Roorda, J. Appl. Phys. **87**, 8504 (2000); **87**, 8513 (2000).
[12] S. W. Chee, P. Krasnochtchekov, and R. S. Averback, J. Appl. Phys. **101**, 014315 (2007).
[13] P. Auric, S. R. Teixeira, B. Dieny, A. Chamberod, and O. Redon, J. Magn. Magn. Mater. **146**, 153 (1995).
[14] *Magnetic Recording Technology*, edited by C. D. Mee and E. D. Daniel (McGraw-Hill, New York, 1995).
[15] X. Jiang, R. Wang, R. M. Shelby, and S. S. P. Parkin, IBM J. Res. Dev. **50**, 111 (2006).
[16] N. Gay–Sanz, C. Prieto, A. Muñoz–Martín, A. de Andrés, M. Vázquez, and S.-C. Yu, J. Mater. Res. **14**, 3882 (1999).
[17] C. Prieto, A. de Bernabé, N. Gay–Sanz, M. Vázquez, and S.-C. Yu, J. Non-Cryst. Solids **246**, 169 (1999).
[18] Y. G. Yoo, S. C. Yu, and W. T. Kim, IEEE Trans. Magn. **31**, 3769 (1995).
[19] Y. G. Yoo, W. T. Kim, S. C. Yu, and Y. D. Kim, J. Magn. Magn. Mater. **157/158**, 233 (1996).
[20] Y. G. Yoo, S. C. Yu, and W. T. Kim, J. Appl. Phys. **79**, 5476 (1996).
[21] S. C. Yu, Y. G. Yoo, W. T. Kim, C. Anderson, D. Dickson, and T. Zeiske, J. Appl. Phys. **81**, 5799 (1997).
[22] I. L. Graff, S. R. Teixeira, L. Amaral, M. C. Martins Alves, and W. H. Flores, J. Appl. Phys. **96**, 1469 (2004).
[23] I. L. Graff, A. Traverse, S. R. Teixeira, and L. Amaral, Nucl. Instrum. Methods Phys. Res. B **249**, 129 (2006).
[24] I. L. Graff, A. Traverse, J. Geshev, S. R. Teixeira, and L. Amaral, Nucl. Instrum. Methods Phys. Res. B **257**, 424 (2007).
[25] J. P. Biersack and L. G. Haggmark, Nucl. Instrum. Methods **174**, 257 (1980); see also http://www.srim.org.
[26] H. Tolentino, D. Z. Cruz, V. Compagnon–Cailhol, E. Tamura, and M. C. Martins Alves, J. Synchrotron Radiat. **5**, 521 (1998).
[27] Web page: http://www.elettra.trieste.it
[28] D. E. Sayers and A. Bunker, *X-ray Absorption: Principles, Applications, Techniques of EXAFS, SEXAFS, and XANES* (Wiley, New York, 1988), p. 211.
[29] B. Ravel and M. Newville, J. Synchrotron Radiat. **12**, 537 (2005).
[30] J. J. Rehr, R. C. Albers, and S. I. Zabinsky, Phys. Rev. Lett. **69**, 3397 (1992).
[31] B. D. Cullity, *Elements of X-ray Diffraction* 2nd ed. (Addison-Wesley, Reading, MA, 1978).
[32] J. J. Rehr and R. C. Albers, Rev. Mod. Phys. **72**, 621 (2000).
[33] T. Nishizawa and K. Ishida, *Binary Alloy Phase Diagrams*, 2nd ed., edited by T. B. Massalski (ASM International, Materials Park, OH, 1996), Vol. 2, p. 1186.
[34] M. Ohring, *The Materials Science of Thin Films* (Academic, New York, 1992).
[35] M. Newville, J. Synchrotron Radiat. **8**, 322 (2001).
[36] E. A. Stern, Phys. Rev. B **48**, 9825 (1993).
[37] V. G. Harris *et al.*, Phys. Rev. B **54**, 6929 (1996).
[38] It is well known that the saturation magnetization (M_s) cannot be precisely

obtained by AGFM measurements, since the amplitude of the output signal depends on the samples' position. Therefore, the samples were measured with a SQUID from zero field up to complete saturation. Afterwards, the AGFM curves were scaled to the actual M_s value estimated from SQUID.

[39]S. Chikazumi, *Physics of Magnetism* (Wiley, New York, 1964).

[40]J. Geshev, A. D. C. Viegas, and J. E. Schmidt, J. Appl. Phys. **84**, 1488 (1998).

[41]Y. Park, S. Adenwalla, G. P. Felcher, and S. D. Bader, Phys. Rev. B **52**, 12779 (1995).

[42]We can have a rough estimation of the Curie temperature by extrapolating the ZFC curve to $M=0$. Of course, to get a precise value, the SQUID measurements have to be done up to higher temperatures, which was not possible in our case.